

## **Sensor and Simulation Notes**

Note 490

April 2004

### **Design and Characterization of a Lens TEM Horn**

W. Scott Bigelow, Everett G. Farr,  
Leland H. Bowen, and Donald E. Ellibee  
Farr Research, Inc.

Dean I. Lawry  
Air Force Research Laboratory / DE

#### **Abstract**

We investigate here a possible method of obtaining smaller UWB antennas with lower sidelobes than those offered by current designs. In support of this, we built and tested a lens TEM horn (lens IRA) employing a polyethylene collimating lens. It was thought that the lens TEM horn, with a more uniformly illuminated aperture field, might lead to higher gain with lower sidelobes than a comparably sized reflector IRA. That hypothesis is tested here. The lens horn, with a 30-centimeter aperture, has a maximum realized gain of 23 dB on boresight at 10 GHz. The normalized antenna impulse response is a clean peak of 35 ps full-width-at-half-maximum (FWHM). For comparison, a highly optimized reflector IRA with 46-cm diameter achieves a maximum realized gain of 28 dB at 19 GHz and exhibits an impulse response of 30 ps FWHM. From theory, we expected the lens horn to exhibit lower sidelobes than the IRA. However, we did not observe that behavior in our experimental model. We suggest additional techniques one might use to reduce the sidelobes in lens TEM horns.

## Table of Contents

<b>Section</b>	<b>Title</b>	<b>Page</b>
1.	Introduction .....	3
2.	Prototype Lens TEM Horn Design .....	4
3.	Testing of the Prototype Lens TEM Horn.....	6
4.	Comparison of the Lens TEM Horn and a Reflector IRA. ....	10
5.	Discussion .....	15
6.	Concluding Remarks .....	17
Appendix A	Lens TEM Horns for Sidelobe Reduction.....	18
Appendix B	Lens Design for the Lens TEM Horn.....	23
References	.....	25

## 1. Introduction

We investigate here the use of lens TEM horns (or lens IRAs) to improve the performance of small UWB antennas. Existing UWB antennas, such as reflector IRAs, have an aperture field distribution that is nonuniform, due to the high concentration of fields near the feed arms. We hypothesize that this leads to higher sidelobes and lower gain than what could be achieved with the more uniform aperture field of a lens TEM horn. The purpose of this project was to build and test a lens TEM horn and attempt to observe this improved performance over a reflector IRA.

There are many possible applications for a small lightweight antenna with high gain and low sidelobes. Such an antenna could improve the performance of UWB radar systems. It might also be useful in an indoor laboratory to make compliance measurements.

A number of earlier efforts have dealt with antennas related to lens TEM horns or lens IRAs. A nine-inch diameter solid dielectric lens IRA was built by Farr and Frost in [1]. Another high-voltage version of a solid dielectric lens IRA with a five-inch diameter was described very recently in [2]. In both of these cases, the antenna was quite heavy, because the feed section was completely embedded in dielectric material. For this project, we wanted the antenna to be as light as possible, so we used an air-filled feed section with a plano-convex lens in the aperture. A third version of a lens TEM horn with an air-filled feed was built by Aurand in [3]. However, that antenna was rather long. For this project, we wanted to minimize the antenna length.

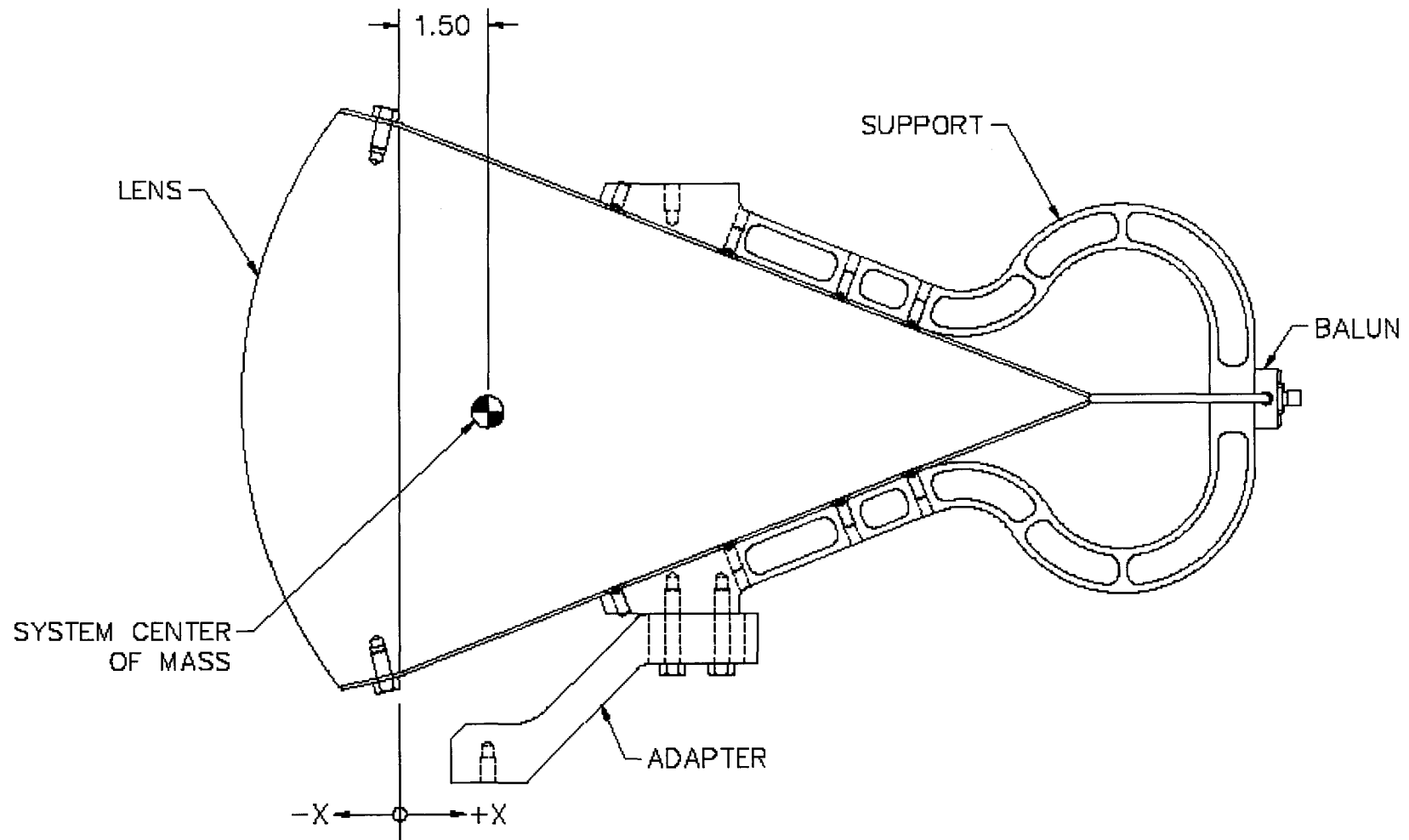
It has been postulated that a lens TEM horn should have lower sidelobes than a reflector IRA, and we advance this argument using both theory and data in Appendix A. In the effort reported here, we built a prototype UWB lens horn and measured its antenna (gain) pattern to characterize its sidelobes. To minimize reflections at the lens-air interfaces, we selected ultra-high-molecular-weight (UHMW) polyethylene, with its relatively low dielectric constant of 2.3, as the lens material. Details of the design and characterization of the prototype lens TEM horn are discussed in the following sections.

## 2. Prototype Lens TEM Horn Design

Our goal was to develop the basic design for a UWB antenna with low sidelobes, high gain, and small size and weight. From prior measurements, we understood the limitations of reflector IRAs for sidelobe reduction, because the aperture fields are high near the feed arms. In contrast, a lens TEM horn has a relatively flat field distribution that tapers off toward the periphery of the aperture. Such an aperture distribution favors low sidelobes. With these considerations in mind, we decided to build a lens TEM horn antenna (or lens IRA) in the form of a flat-plate TEM horn with a collimating lens. By focusing the radiated field, the lens permits a compact, relatively high gain design.

For our prototype lens TEM horn design, shown in Figure 1, we selected an aperture diameter of 30 cm. Our choice of a  $200\ \Omega$  horn geometry with a  $F/D$  ratio of 1.0 led to a horn-opening angle of 42.6 degrees. The input impedance was matched by our standard splitter/balun to a  $50\ \Omega$  feed. For the lens, we chose UHMW polyethylene with a dielectric constant of 2.3. The collimating lens was plano-convex, with the spherical surface facing forward and with the flat surface co-planar with the horn aperture. The curvature of the lens placed its focus at the feed point of the horn. In Appendix B, we present expressions which parameterize the radius of curvature of the lens and its thickness by the index of refraction and aperture radius.

Not shown in Figure 1 are optional diffraction-reducing lips with a radius of curvature of 1.32 cm, which could be mounted at the open end of each feed arm. Also not shown in Figure 1 is a pair of  $400\ \Omega$  resistor strings, which could be used in parallel to terminate the horn aperture at  $200\ \Omega$ . Note also that Figure 1 shows a slight bend in the feed arms where they make first contact with the lens. The actual device tested here had flat feed arms.



5

Figure 1. Design for a prototype lens TEM horn employing a polyethylene collimating lens. Diffraction-reducing lips, used in some measurements, are not shown. The mounting adapter was not used. Instead, a standard tripod mount interfaced to an antenna positioner.

### 3. Testing of the Prototype Lens TEM Horn

The lens TEM horn was tested at our outdoor antenna range. The range employed the PSPL 4015C pulser driving a calibrated Farr Research  $50\ \Omega$  TEM horn as transmitter. The receiving lens horn antenna was mounted on a computer-controlled AZ-EL positioner. The received impulse response was detected by an 80E04 sampling module driving a Tektronix TDS 8000 digital sampling oscilloscope. The entire process, including positioner orientation and data acquisition and storage, was under control of the Farr Research *PATAR*<sup>TM</sup> (Portable Automated Time-domain Antenna Range) system.

#### 3.1 Lens TEM Horn Test Configurations

We tested the lens TEM horn in four configurations: (1) the bare TEM horn with no focusing lens at the aperture, (2) the basic configuration, including the aperture lens, (3) the basic configuration, with diffraction-reducing lips added at the feed arm aperture, and (4) the basic configuration with impedance-matching resistors terminating the aperture. In Figure 2, we show

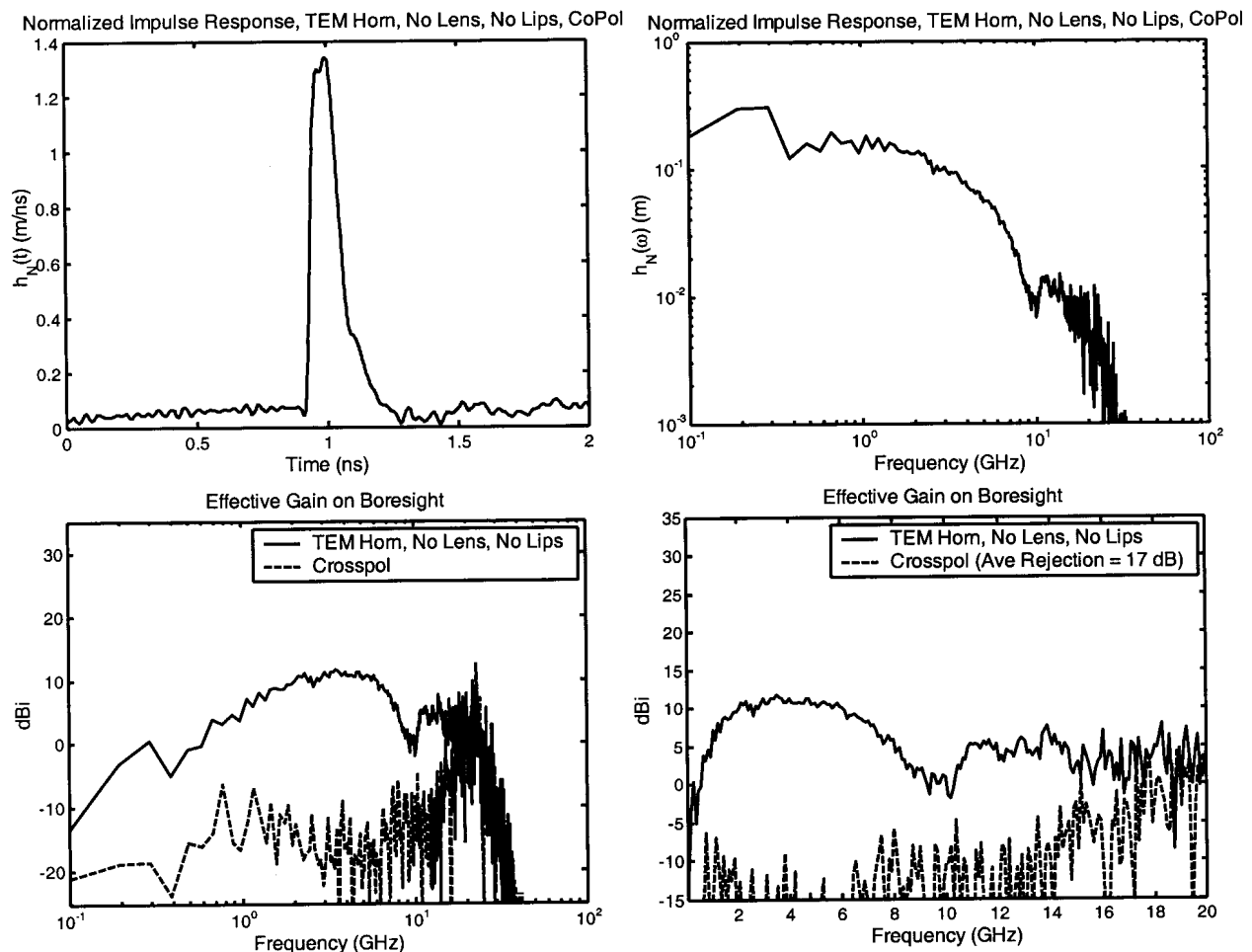


Figure 2. Normalized impulse response and realized gain on boresight for the TEM horn without its collimating lens.

the impulse response and realized gain on boresight for the first configuration, the bare TEM horn. These data demonstrate that the collimating lens plays a crucial role in the performance of the prototype antenna. Without the lens to focus the radiation, the duration (FWHM) of the impulse response is about 118 ps; there is little frequency content beyond 10 GHz; and the maximum gain on boresight is only about 10 dB. Although not shown here, the gain is highest in off-boresight directions, except at the lowest frequencies.

The utility of the diffraction-reducing lips is questionable when compared to the basic lens horn configuration. We observed only a 1 dB increase in peak gain on boresight with the lips. It may be that the lips with their 1.32 cm radius of curvature are simply too small to have a significant impact on the lens horn performance.

The fourth configuration, the lens horn with resistive aperture termination, has been tested only in the laboratory, where we measured the impact the termination on the TDR and on the derived  $S_{11}$  parameter. For these measurements, the horn was terminated in its characteristic  $200 \Omega$  impedance by a pair of  $400 \Omega$  resistor strings applied in parallel between the feed plates at each side of the aperture. The impact of the termination is demonstrated in Figure 3.

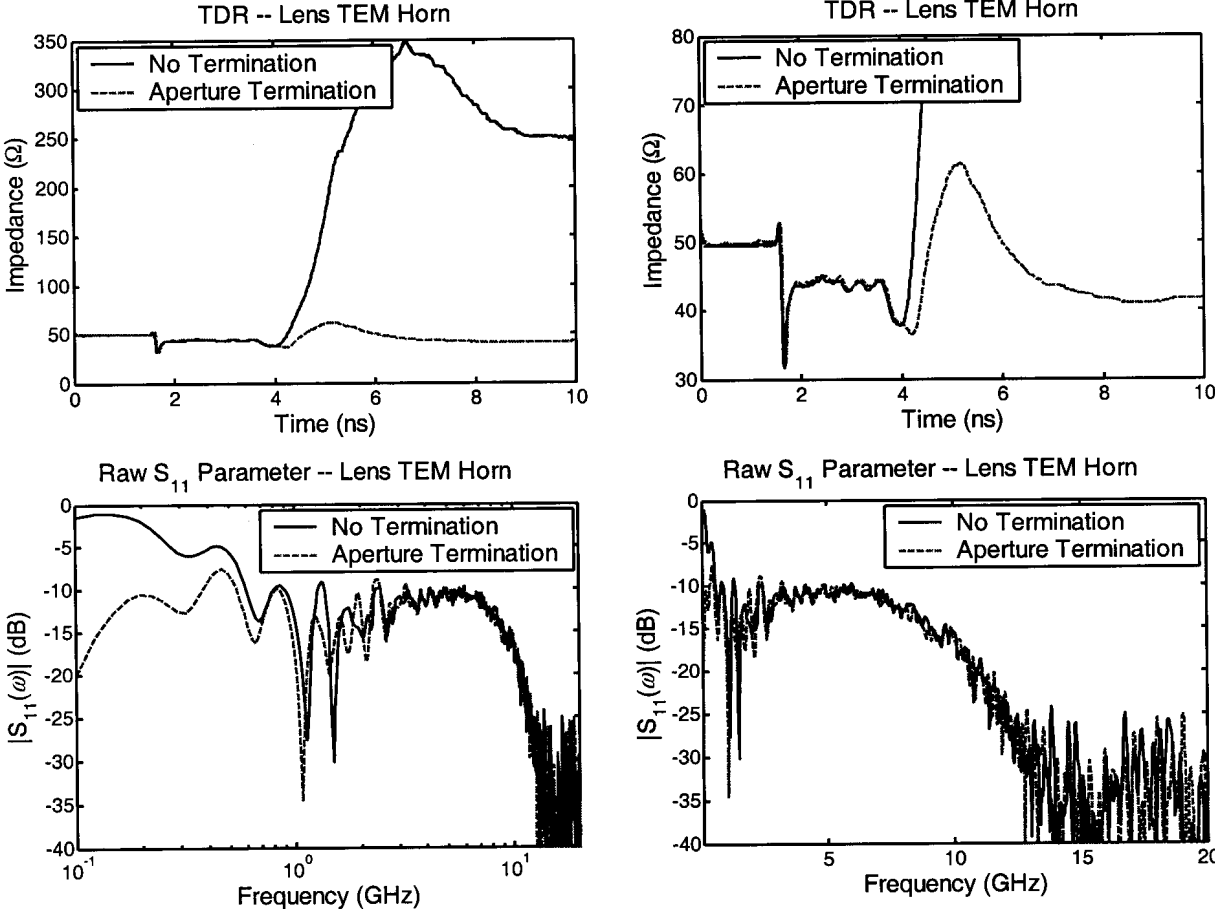


Figure 3. Effect of an impedance-matching  $200 \Omega$  aperture termination on the TDR and on the magnitude of the raw (not corrected for cable loss)  $S_{11}$  parameter of the lens TEM horn.

We observe that the open circuit impedance at the end of the horn is reduced by a factor of about 30 with the resistors in place. This represents an improvement in the low-frequency impedance match at the aperture. Below 500 MHz, the raw  $S_{11}$  magnitude (not corrected for cable loss) is reduced by 3–20 dB. There is no significant effect of the termination above 2 GHz. Although the terminated horn has not been tested on the range in transmission/reception, we expect no substantial impact on either sidelobes or boresight gain above 2 GHz. Note that the preferred method of terminating a TEM horn is to feed the resistance back to the feed point of the horn, as described in [4,5]. Doing so preserves the low-frequency portion of the radiated field.

### 3.2 Analysis of the Time Domain Range Measurements

We now present performance data for the basic lens TEM horn configuration, without diffraction-reducing lips, and without aperture termination. The presentation includes a photo of the horn along with its normalized impulse response (Figure 4), a TDR measurement of the horn and resulting magnitude of the  $S_{11}$  parameter (Figure 5), the realized co- and cross-polarized boresight gain (Figure 6), and co-polarized gain patterns in H-plane (azimuth) and E-plane (elevation), normalized to boresight gain (Figure 7).

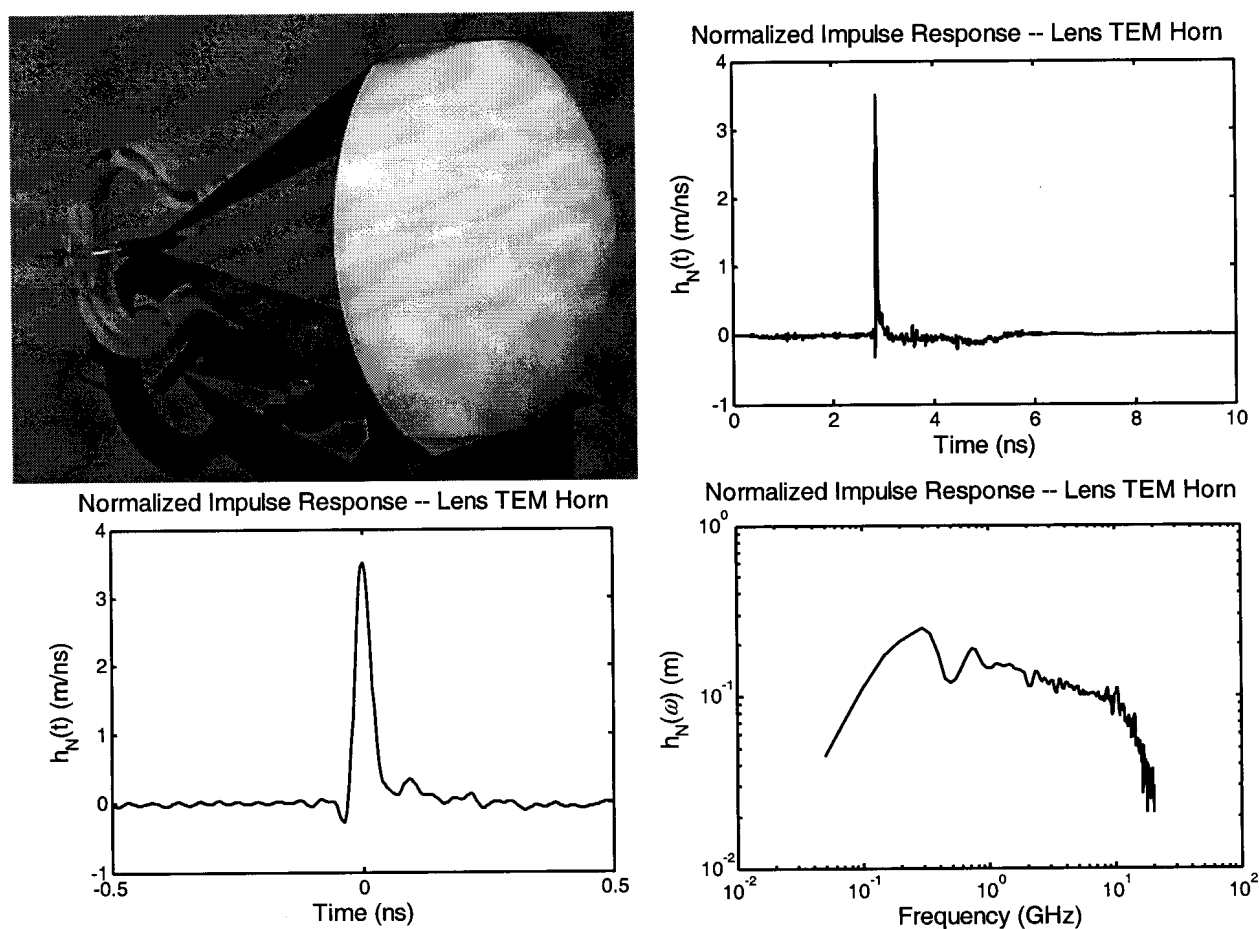


Figure 4. Lens TEM horn photo and normalized impulse response on boresight. The time domain duration of the response is 35 ps (FWHM). There is significant frequency content up to about 20 GHz.

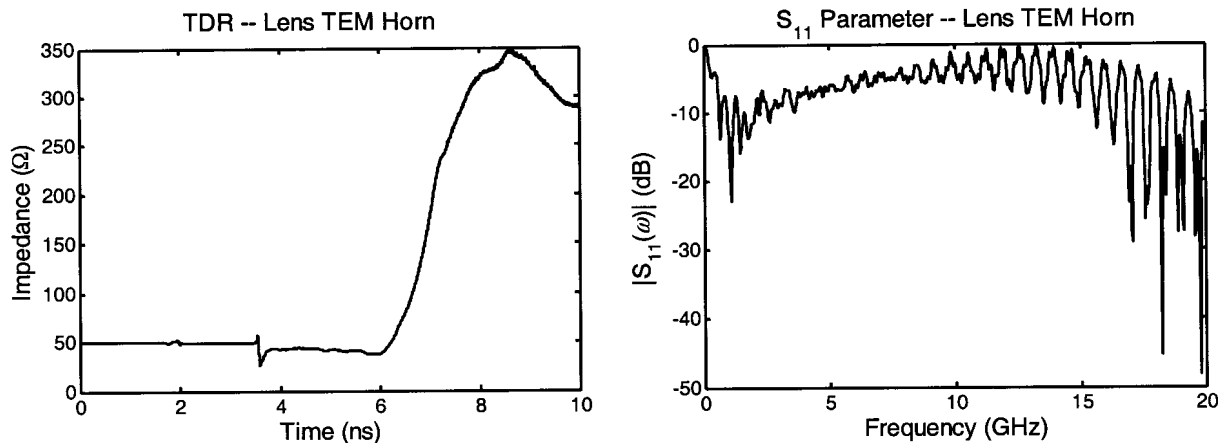


Figure 5. TDR measurement of the lens TEM horn and the magnitude of the corresponding  $S_{11}$  parameter, corrected for cable loss. In the feed arm region extending from about 3.5 ns to 6 ns, the impedance is only  $45 \Omega$ . The arm width at the aperture would have to be reduced by approximately 2 cm to raise the impedance to the  $50 \Omega$  design level.

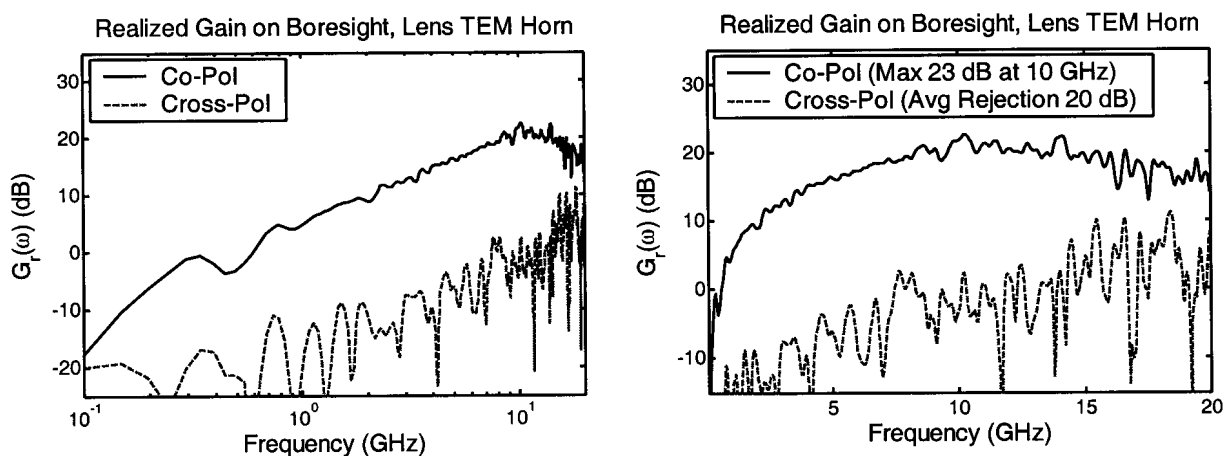


Figure 6. Realized co- and cross-polarized gain on boresight for the lens TEM horn.

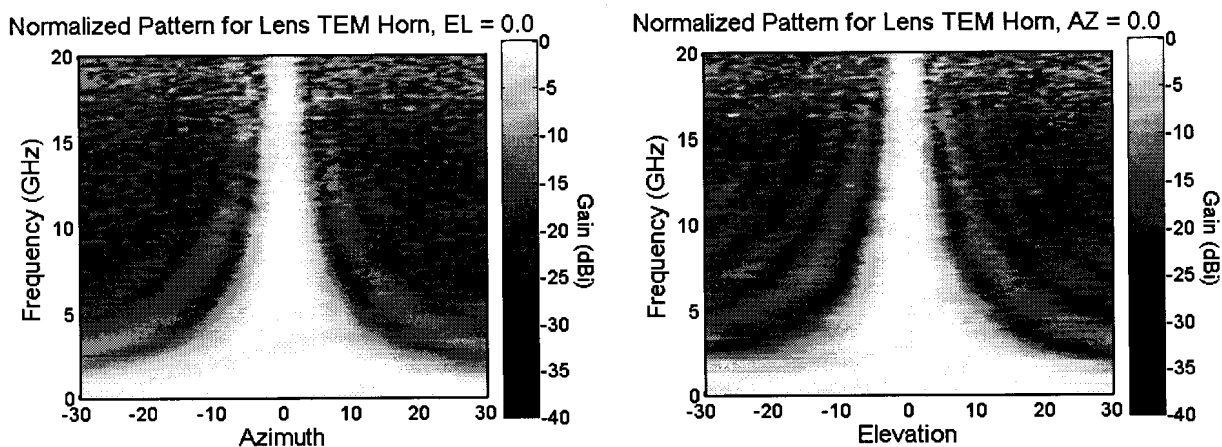


Figure 7. Gain patterns for the lens TEM horn in the H-plane (left) and E-plane (right), normalized to the boresight gain.

#### 4. Comparison of the Lens TEM Horn and a Reflector IRA.

We compare here the performance of the 30-cm lens TEM horn without resistive loading to that of a 46-cm Farr Research reflector IRA-3, shown in Figure 8. The results of the comparison on boresight are shown in Figure 9, where we observe that the smaller horn has a normalized impulse response that is down by nearly a factor of two and boresight gain that is down by about 4 dB from that of the reflector IRA over a broad frequency range. In addition, the high-end rolloff begins at a lower frequency in the lens horn—around 10 GHz instead of 18 GHz. The return loss ( $S_{11}$ ) comparison is shown in Figure 10, where we see that the return loss for the lens TEM horn is much higher (worse) than that of the reflector IRA. Antenna pattern data is shown in Figure 11, Figure 12, and Figure 13, where we observe that the sidelobe levels of the lens horn are higher than those of the IRA-3.



Figure 8. Farr Research IRA-3.

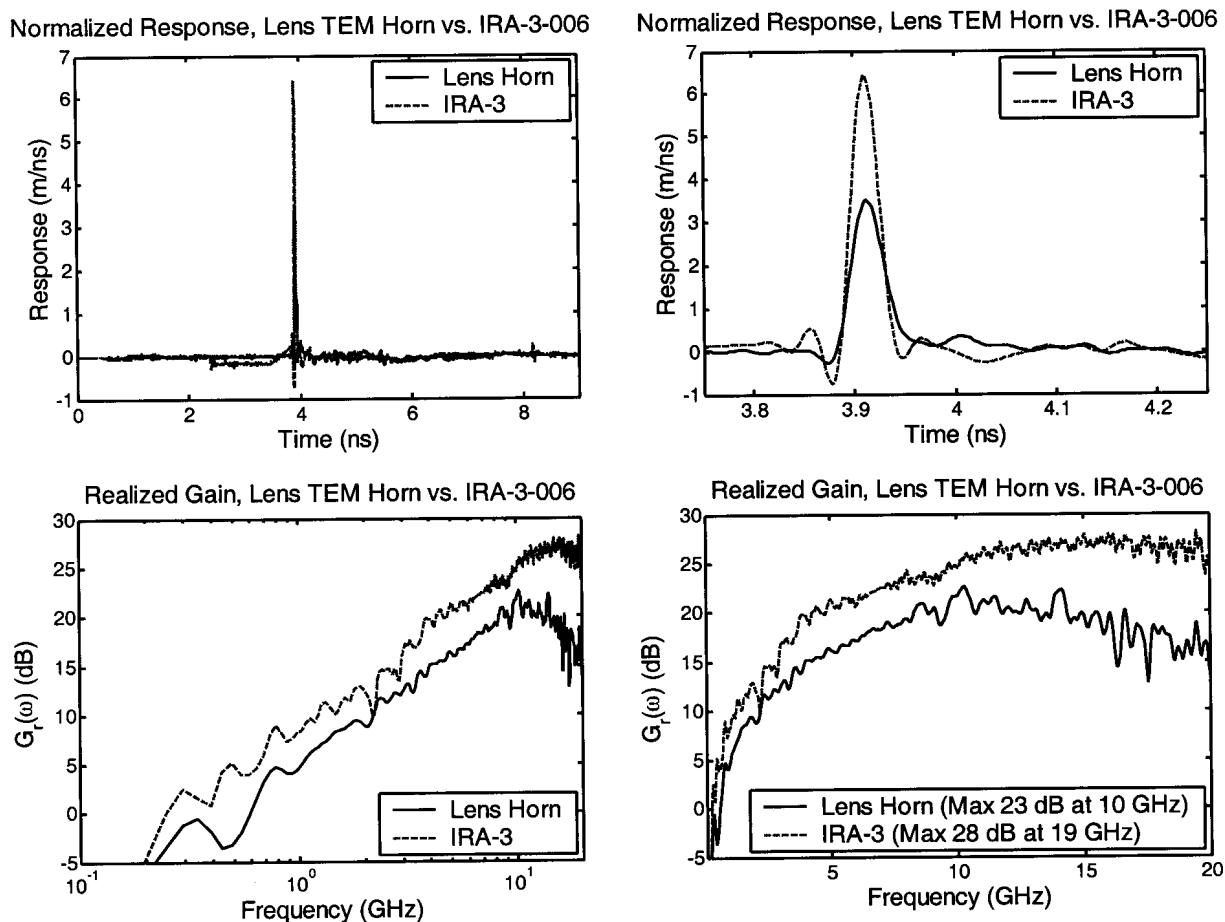


Figure 9. Comparison of normalized impulse response (top) and realized gain on boresight (bottom) for the lens TEM horn and the IRA-3.

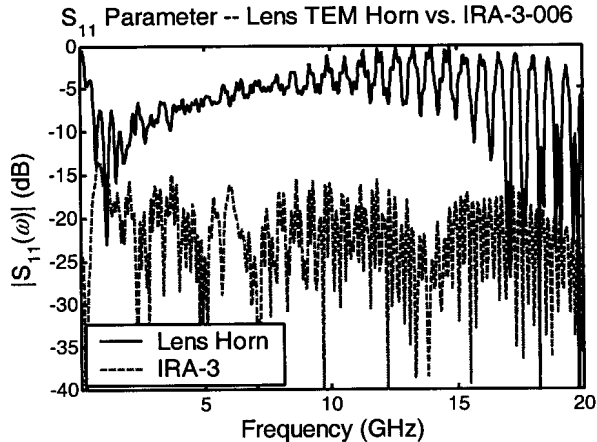
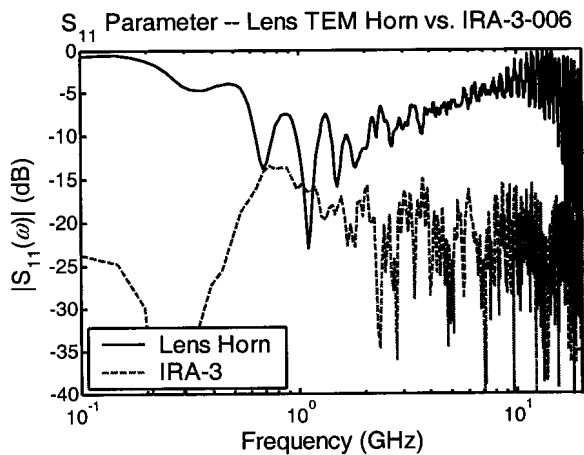


Figure 10.  $S_{11}$  parameter comparison for the lens TEM horn and IRA-3.

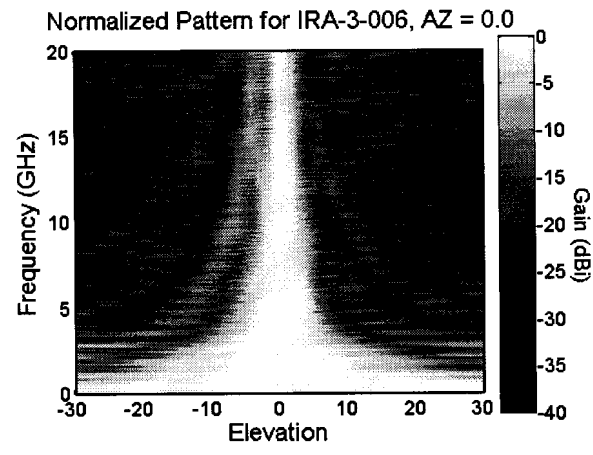
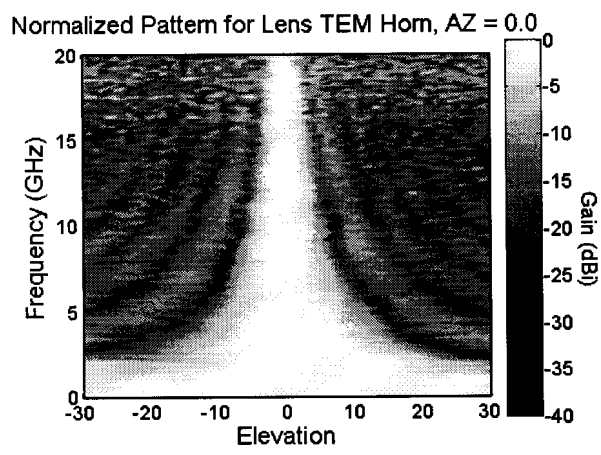
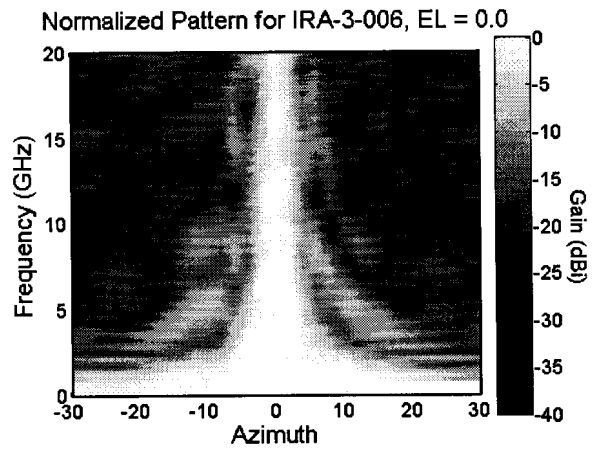
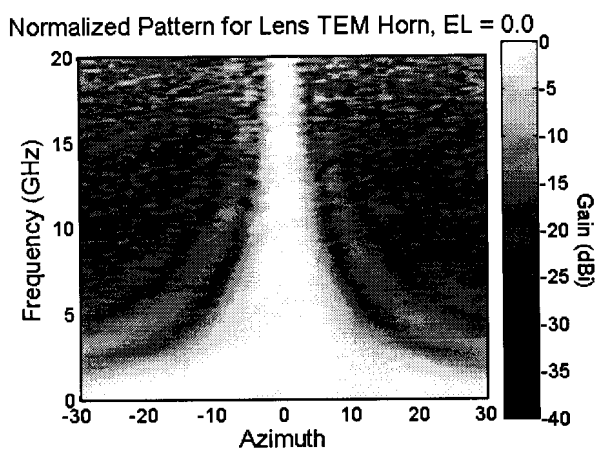
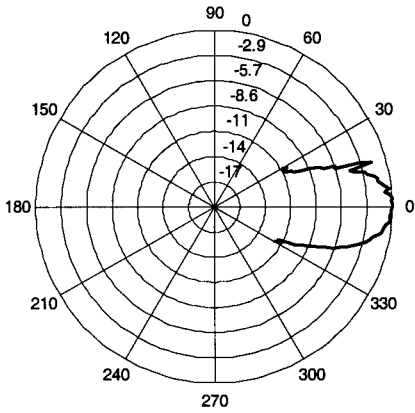
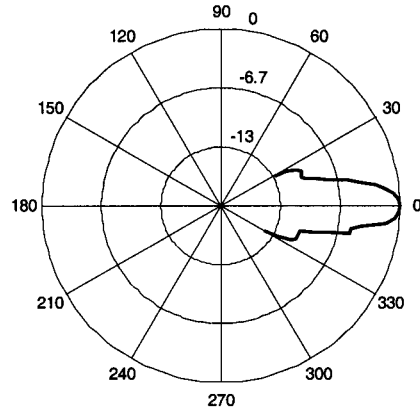


Figure 11. Comparison of normalized gain patterns in the H-plane (top) and E-plane (bottom) for the lens TEM horn and IRA-3.

Normalized Pattern for Lens TEM Horn



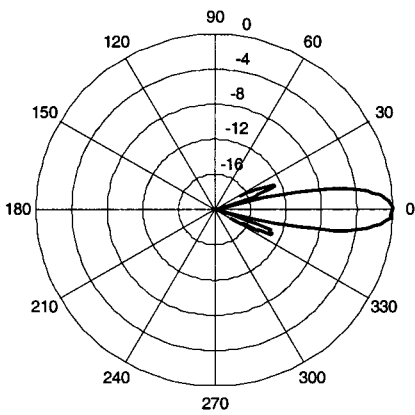
Normalized Pattern for IRA-3-006



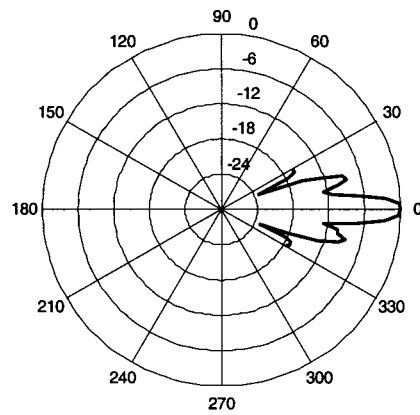
Gain (dBi) at 2.000 GHz vs. Azimuth, EL = 0.0

Gain (dBi) at 2.000 GHz vs. Azimuth, EL = 0.0

Normalized Pattern for Lens TEM Horn



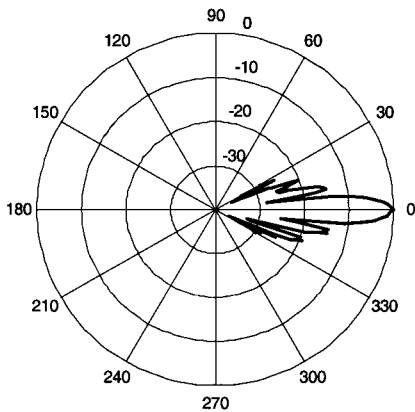
Normalized Pattern for IRA-3-006



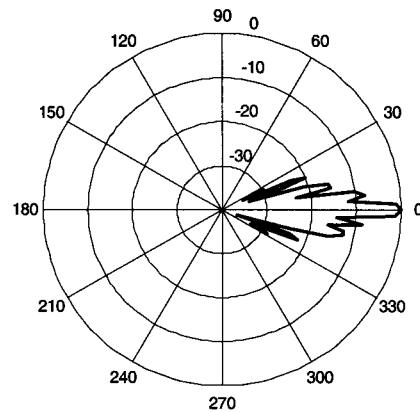
Gain (dBi) at 4.000 GHz vs. Azimuth, EL = 0.0

Gain (dBi) at 4.000 GHz vs. Azimuth, EL = 0.0

Normalized Pattern for Lens TEM Horn



Normalized Pattern for IRA-3-006

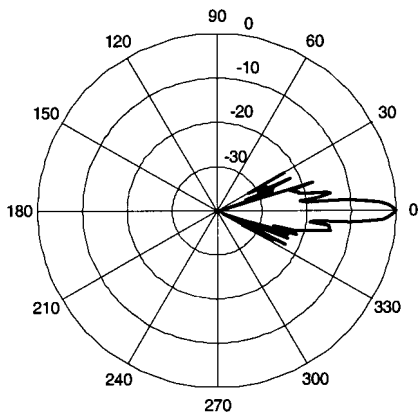


Gain (dBi) at 8.000 GHz vs. Azimuth, EL = 0.0

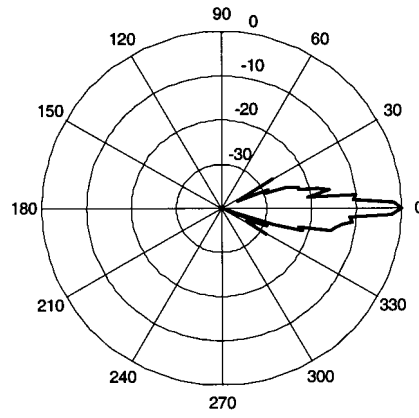
Gain (dBi) at 8.000 GHz vs. Azimuth, EL = 0.0

Figure 12. Comparison of normalized gain pattern frequency cuts in the H-plane for the lens TEM horn and IRA-3. (Continued below.)

Normalized Pattern for Lens TEM Horn



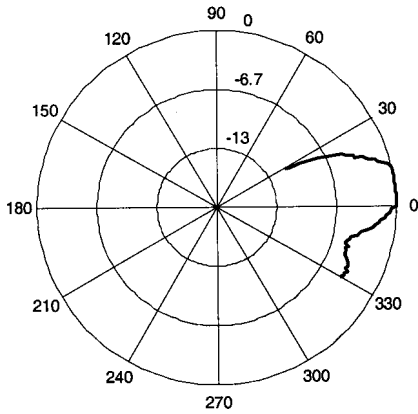
Normalized Pattern for IRA-3-006



Gain (dBi) at 10.000 GHz vs. Azimuth, EL = 0.0      Gain (dBi) at 10.000 GHz vs. Azimuth, EL = 0.0

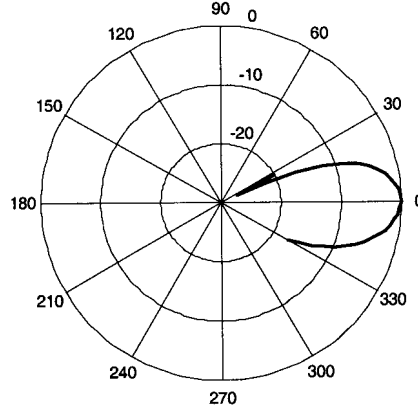
Figure 12. Comparison of normalized gain pattern frequency cuts in the H-plane for the lens TEM horn and IRA-3.

Normalized Pattern for Lens TEM Horn



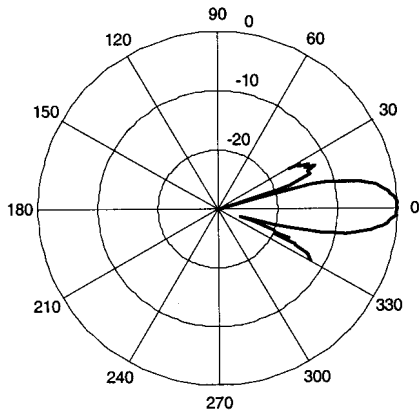
Gain (dBi) at 2.000 GHz vs. Elevation, AZ = 0.0

Normalized Pattern for IRA-3-006



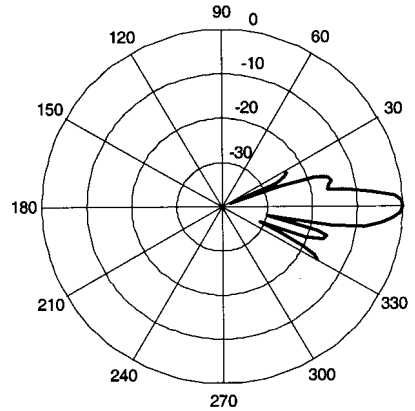
Gain (dBi) at 2.000 GHz vs. Elevation, AZ = 0.0

Normalized Pattern for Lens TEM Horn



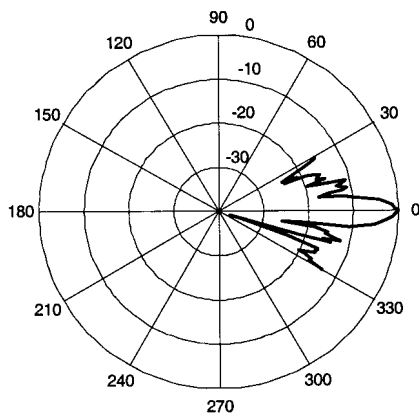
Gain (dBi) at 4.000 GHz vs. Elevation, AZ = 0.0

Normalized Pattern for IRA-3-006



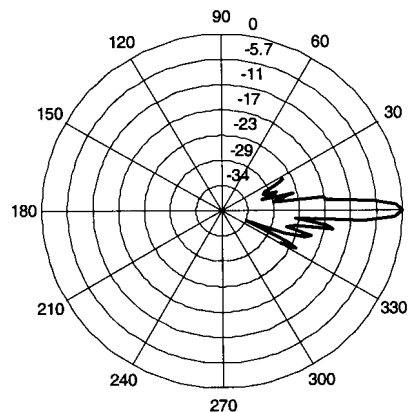
Gain (dBi) at 4.000 GHz vs. Elevation, AZ = 0.0

Normalized Pattern for Lens TEM Horn



Gain (dBi) at 8.000 GHz vs. Elevation, AZ = 0.0

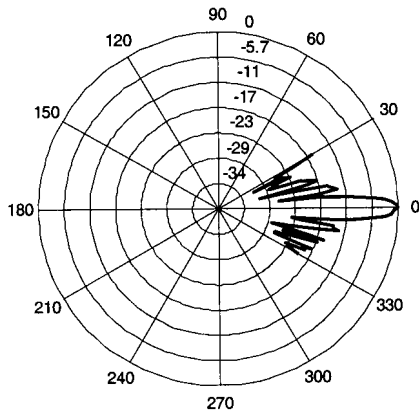
Normalized Pattern for IRA-3-006



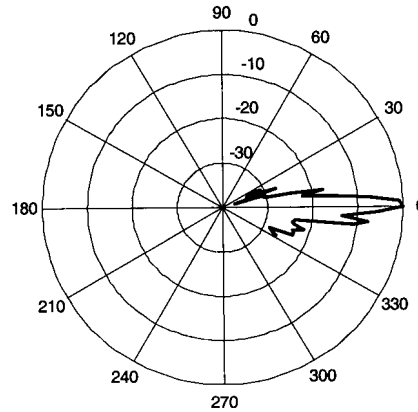
Gain (dBi) at 8.000 GHz vs. Elevation, AZ = 0.0

Figure 13. Comparison of normalized gain pattern frequency cuts in the E-plane for the lens TEM horn and IRA-3. (Continued below.)

Normalized Pattern for Lens TEM Horn



Normalized Pattern for IRA-3-006



Gain (dBi) at 10.000 GHz vs. Elevation, AZ = 0.0      Gain (dBi) at 10.000 GHz vs. Elevation, AZ = 0.0

Figure 13. Comparison of normalized gain pattern frequency cuts in the E-plane for the lens TEM horn and IRA-3.

## 5. Discussion

We had hoped that the more uniform aperture field of the lens TEM horn would lead to better performance than a reflector IRA; but, in a number of ways, the lens TEM horn fell short of our expectations. First, we had hoped that the lens TEM horn would have a higher realized gain than a reflector IRA of similar size. The reflector IRA, with a diameter of 46 cm, had about a 4-dB advantage in realized gain over the lens horn, with a diameter of 30 cm. The size difference accounts for 3.7 dB of gain difference, calculated by converting the ratio of the diameters to decibels. Thus, a reflector IRA with the same diameter still would have slightly outperformed the lens horn by about 0.3 dB. Second, the FWHM of the normalized antenna impulse response (NAIR) of the lens horn (35 ps) was larger than that of the reflector IRA (30 ps). Third, the peak magnitude of the NAIR for the lens horn was only about half that of the reflector IRA. Fourth, the sidelobe levels of the lens horn were higher than those of the reflector IRA. Fifth, the return loss of the lens horn was much higher than that of the reflector IRA. Finally, the high-end gain of the lens horn starts to roll off at 10 GHz, as compared to 18 GHz for the reflector IRA.

There are several possible reasons for the disappointing performance of the lens TEM horn. First, the feed impedance of the lens horn was not exactly 200 ohms, but around 180 ohms. Our guess is that this is a rather minor effect. Second, the curved surface of the plano-convex lens was spherical and designed using a paraxial approximation. This approximation was used in place of a numerically designed surface calculated by time-of-flight. Spherical aberration in the current lens causes a spread of about 18 ps in the arrival times of rays within the focused output of the horn. This is fairly small compared to the 35-ps FWHM, but perhaps it is significant.

Probably the most important reason for the modest performance of the lens horn lies in its high return loss, which reduces the realized gain. Portions of this return loss are due to the two air-dielectric interfaces in the lens. However, the reflections from the large impedance discontinuity at the feed point are probably more significant. The feed point discontinuity is largely due to neglect of the finite feed arm thickness when compared to the feed point gap. This effect, which may significantly impact the high-frequency performance of the lens horn, can be reduced by improved feed point design and by practice in fabrication. Commercially available reflector IRAs have about a 10% deviation in impedance from 50 ohms at the feed point, but the lens IRA discussed here has about twice that. The feed point of reflector IRAs might be expected to be more difficult to build than that of lens horns, because they have four feed arms coming together instead of only two plates. This gives us some hope that, with a few iterations, the feed point problem can be remedied.

The FWHM of 35 ps for the lens horn compares somewhat modestly to earlier lens horn designs built by others. Both Aurand [3] and Farr and Frost [1] built lens TEM horns for which they reported a FWHM of around 20 ps. The Aurand design had the same diameter as the current design, but their horn was longer and had smaller opening angles. In Aurand's design, the plate-opening angle was  $9^\circ$  and the plate-width angle was  $23^\circ$ . In the current design, the plate-opening angle is  $46^\circ$  and the plate-width angle is  $30^\circ$ . The larger opening angles of our design make it more difficult to maintain a fast risetime. To a certain degree, this effect was expected, because we wanted to build a more compact antenna, but we did not expect the effect would be so large. The solid dielectric lens IRA built by Farr and Frost [1] had a 23-cm diameter, instead of 30 cm, so the smaller aperture made it easier to maintain a fast risetime. In addition, the Farr and Frost design had only a single air-dielectric interface that could cause reflections. Furthermore, the shape of the air-dielectric interface in the solid design is an exact prolate spheroid, requiring no approximations. However, a big disadvantage of the solid design is that it is much heavier than the current design.

Our measurements clearly demonstrated that inclusion of the collimating lens was crucial to achieving adequate UWB performance at frequencies above a few gigahertz. For a low-frequency application, the lens may be unnecessary. Evidence to support the use of diffraction-reducing lips at the mouth of the horn was inconclusive, due to the small size of the lips that were tested. The potential benefits of larger lips merit further investigation. Termination of the aperture at the characteristic impedance of the horn improved the impedance match and return loss at frequencies below 500 MHz. However, no significant impact was observed above about 2 GHz.

## 6. Concluding Remarks

We built a lens TEM horn, or lens IRA, with the intention of developing a compact antenna with high gain and a low sidelobe level. We had expected that the more uniform aperture field of the horn would provide improved performance when compared to a reflector IRA. However, the performance of the lens horn fell short of our expectations with respect to boresight gain, sidelobe level, return loss, and FWHM of the normalized antenna impulse response. This may be due to approximations in the feed point and lens designs and/or the short length of the horn.

We also compared the response of our lens horn to other lens horns, and we found that the others had faster impulse responses. However, previous lens horns benefited either by allowing a longer horn, or by having a solid dielectric feed section, which eliminated approximations in the lens design.

There are several paths which future investigations might follow in an attempt to remedy this outcome. Aperture potentials should be used to calculate the far field, as suggested in Appendix A, to quantify our prediction of lower sidelobes. Next, the lens design based on the paraxial optics approximation might be replaced with a more accurate design based on equal time-of-flight for all ray paths, and the feed point design could be improved by accounting for the finite thickness of the feed arms. Finally, absorbers could be used at the exposed sides of the feed arms to help isolate sources of sidelobe radiation..

The aperture treatments explored here had minimal impact on lens TEM horn performance. Aperture termination of the horn in its characteristic  $200\ \Omega$  impedance improved the low-frequency impedance match, greatly reducing the low-frequency return loss. However, there was no appreciable effect above 2 GHz. The small diffraction-reducing lips (1.32 cm radius of curvature) had no appreciable impact on the TDR measurement, return loss, boresight gain, or gain pattern. These lips may simply have been too small to be effective. In the future, the use of larger aperture lips should be investigated (e.g., lips with 5–10 cm radius of curvature). However, larger lips would reduce the benefit of having a small aperture.

## Acknowledgment

We wish to thank the Air Force Research Laboratory, Directed Energy Directorate, for funding this work.

## Appendix A Lens TEM Horns for Sidelobe Reduction

We propose here an argument for why a lens TEM horn (lens IRA) should have lower sidelobes than a reflector IRA.

First, let us consider the aperture potential of a focused antenna, as developed by Farr in [6]. The normalized aperture potential,  $\Phi^{(e)}(y)$  and  $\Phi^{(h)}(x)$ , is defined as

$$\begin{aligned}\Phi^{(h)}(x) &= \frac{-1}{V} \int_{C_1(x)} E_y dy \\ \Phi^{(e)}(y) &= \frac{-1}{V} \int_{C_2(y)} E_y dx\end{aligned}\tag{A.1}$$

The contours  $C_1(x)$  and  $C_2(y)$  are defined in Figure A.1. The aperture potentials are proportional to the radiated field in the principal planes [6, 7]

$$\begin{aligned}\bar{E}^{(h)}(r, t) &= \bar{1}_y \left( \frac{-V}{r} \right) \frac{\cot(\theta)}{2\pi} \Phi^{(h)} \left( \frac{ct}{\sin(\theta)} \right) \\ \bar{E}^{(e)}(r, \theta, t) &= \pm \bar{1}_\theta \left( \frac{-V}{r} \right) \frac{1}{2\pi \sin(\theta)} \Phi^{(e)} \left( \frac{ct}{\sin(\theta)} \right)\end{aligned}\tag{A.2}$$

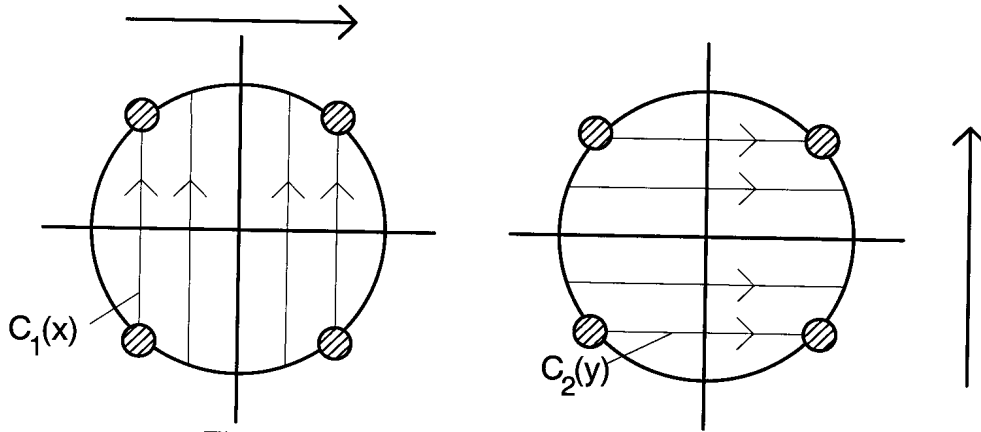


Figure A.1. Locations of  $C_1(x)$  and  $C_2(y)$ .

To achieve low sidelobes, we want the normalized potentials to be constant in the center, and taper to zero at the edge. This would mimic the classical edge taper that is commonly used in the frequency domain world.

Let us consider now the aperture field of the lens TEM horn. A sketch of the lens TEM horn is shown in Figure A.2. Its normalized potentials are shown in Figure A.3 for both the E-

and H-planes. Due to symmetry, the potential functions are the same in both planes for the case where the impedance is  $377 \Omega / 2$ . The normalized aperture potential for the lens TEM horn is a good approximation to the preferred behavior—flat in the middle and tapered at the edge.

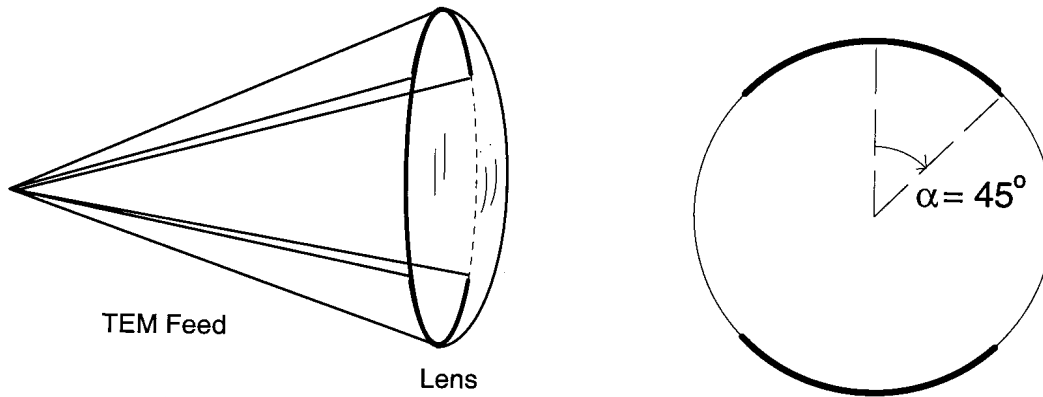


Figure A.2. Sketch of a lens TEM horn (Lens IRA).

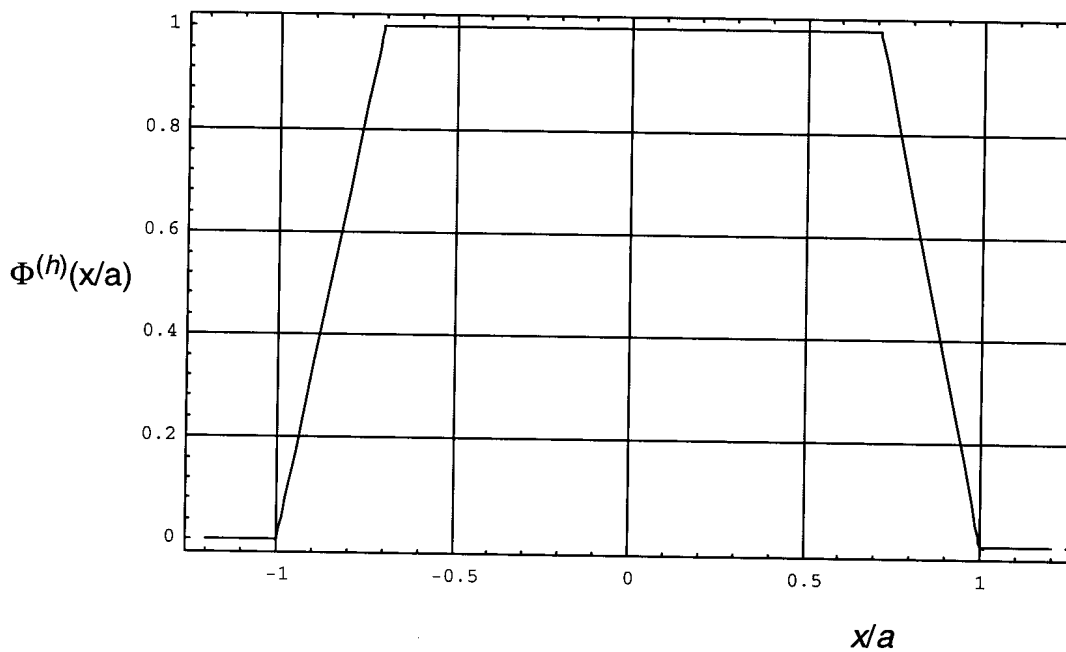


Figure A.3. Plot of the normalized potential function,  $\Phi^{(h)}(x)$ . The normalized potential function,  $\Phi^{(e)}(y)$ , has the same shape due to symmetry in horns with impedance of  $377 \Omega / 2$ .

Let us now consider a reflector IRA. The aperture for a reflector IRA is shown in Figure A.4, and its normalized potential functions are shown for the H-plane in Figure A.5, and for the E-plane in Figure A.6. We can see that both of these functions differ greatly from the preferred aperture distribution (flat in the center and tapered at the edge). The behavior in the H-plane is, in fact, differs significantly from our preferred distribution.

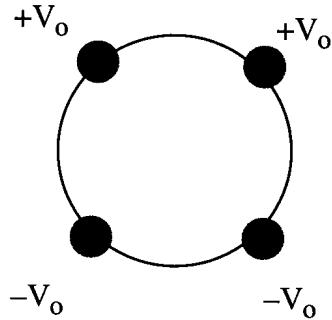


Figure A.4. The aperture for a four-wire reflector IRA.

It is possible to convert the normalized aperture distributions to frequency domain pattern plots. Examples of these pattern plots for measured data are shown in Figure A.7. It should be straightforward to convert our theoretical normalized aperture potentials to pattern plots. We expect that such calculations would demonstrate that a smoother aperture with a tapered edge yields a pattern with lower sidelobes. Thus, the lens TEM horn seems to be the preferred design to achieve low sidelobes.

Note also that of the two normalized potential functions for the reflector IRA, the H-plane potential function is the less well-behaved. By that, we mean that it differs more from the preferred shape (constant in the middle, tapered at the edge) than the normalized E-plane potential. We find this interesting because the measured H-plane pattern exhibits worse sidelobes than the E-plane pattern in Figure A.7. This tends to support the hypothesis that lens TEM horns should have lower sidelobes than reflector IRAs.

Thus, we see that there is a considerable body of evidence that suggests that lens TEM horns should have lower sidelobes than reflector IRAs. To confirm this, we should eventually carry out a series of calculations to convert normalized potentials to antenna patterns.

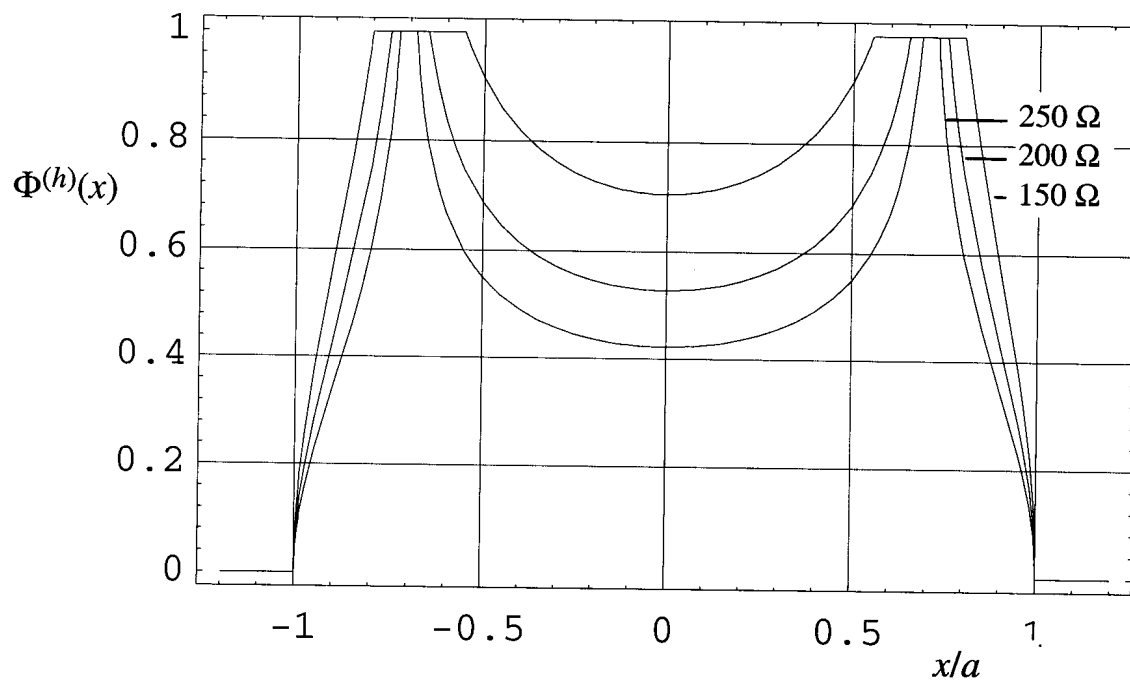


Figure A.5. The normalized potential function,  $\Phi^{(h)}(x)$ , in a reflector IRA for a few different impedances.

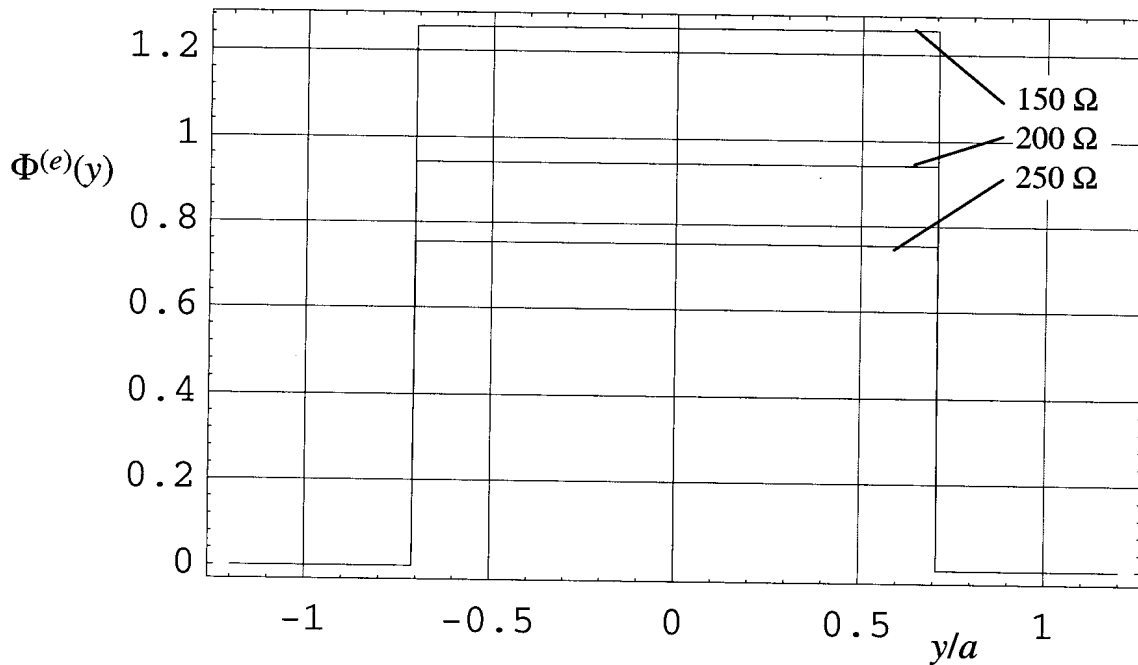


Figure A.6. The normalized potential function,  $\Phi^{(e)}(y)$ , in a reflector IRA for a few different impedances.

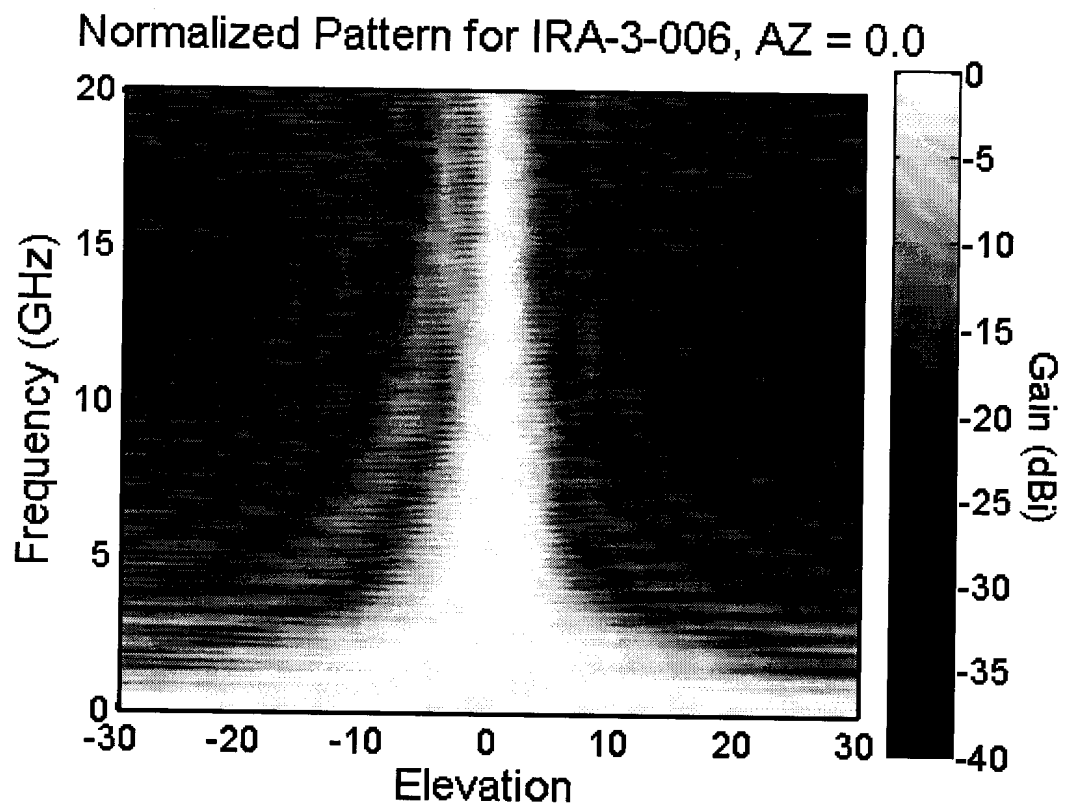
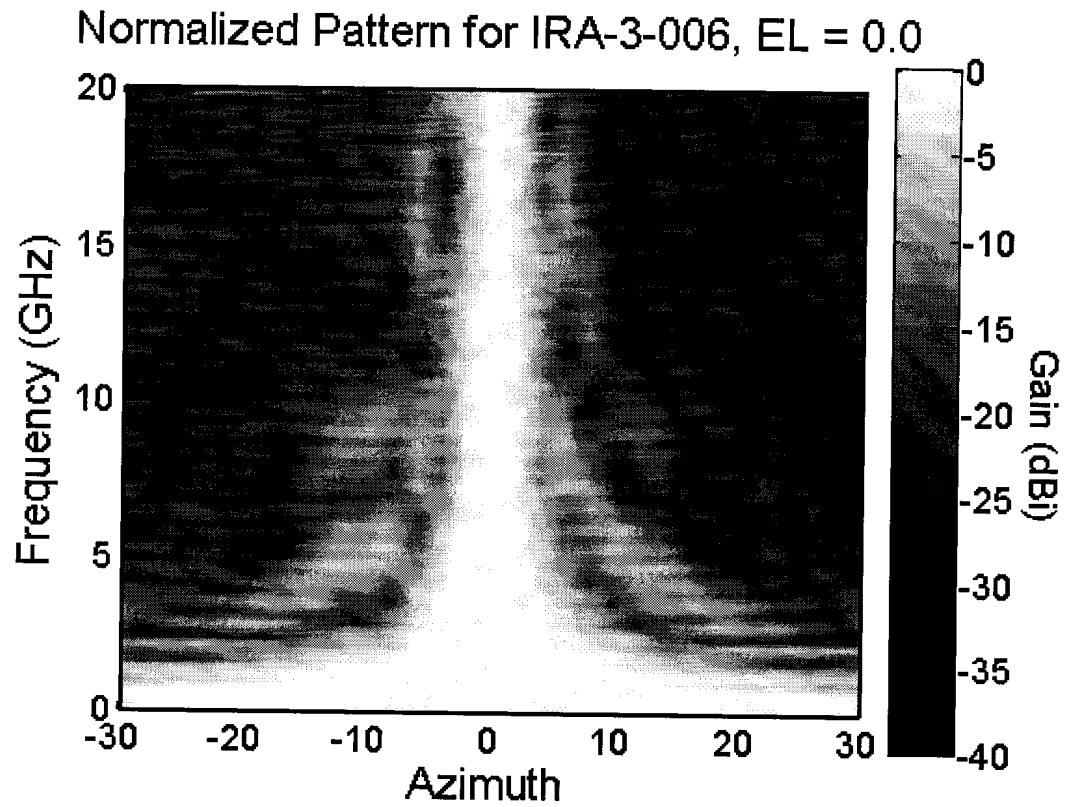


Figure A.7. Measured pattern plots for the IRA-3 in the E-plane (top) and H-plane (bottom).

## Appendix B

### Lens Design for the Lens TEM Horn

We present here our derivation of the radius of curvature and thickness of a spherical planar-convex collimating lens for the lens TEM horn. The derivation is based on the assumptions of paraxial geometric optics. Although those assumptions are violated by our  $F/D = 1$  horn, they lead to a particularly simple lens design, which we opted to investigate before resorting to a more exact time-of-flight design.

The geometry of the lens horn is indicated in Figure B.1. The horn has an aperture diameter,  $D$ , and focal length,  $F$ , of  $2a_0$ . The lens is assumed to be constructed from a uniform, lossless dielectric material with index of refraction,  $n = \epsilon_r^{1/2}$ . The flat surface of the lens is coplanar with the aperture of the horn and has the same radial dimension. On its optical axis, the thickness of the lens is  $d$ . The radius of curvature of the spherical surface is  $r$ . We complete our specification of the lens by requiring that its focal point coincide with the feed point of the horn.

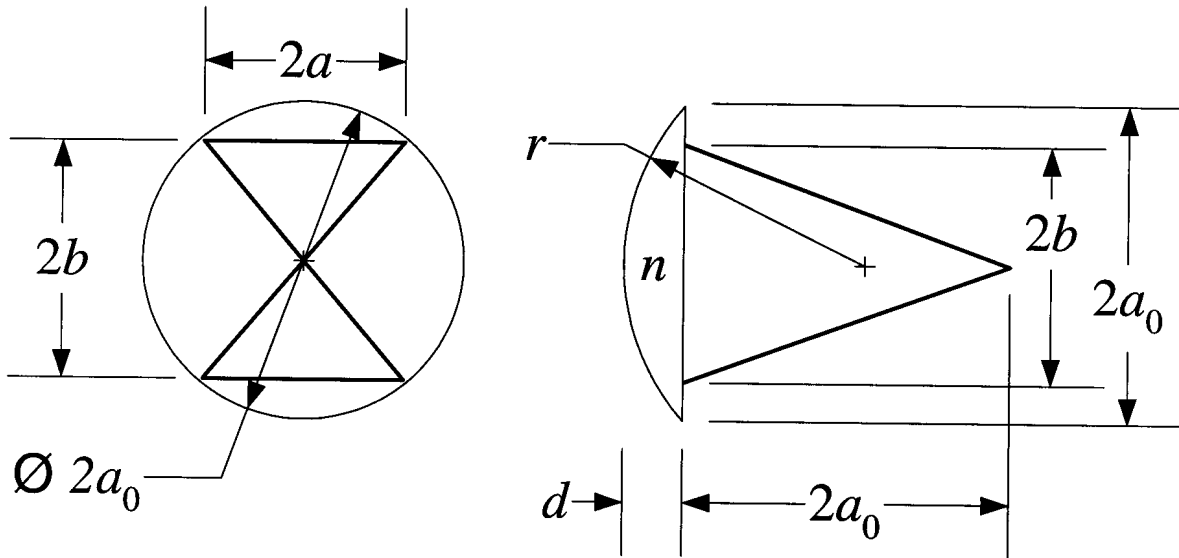


Figure B.1. Diagram of the lens TEM horn antenna.

At the aperture of the horn, the flat feed plates have a width of  $2a$  and separation of  $2b$ . As shown in [8, 9, 10], the ratio of the separation to the width,  $b/a$ , is the primary determinant of the characteristic impedance of the horn. However, neither this ratio nor the plate widths themselves enter into the lens design expressions. Indeed, given our assumptions, the design parameters of radius of curvature and thickness are completely determined by the index of refraction of the lens,  $n$ , and by its aperture radius,  $a_0$ .

We begin by obtaining an expression for the thickness of the lens in terms of its radius of curvature and aperture radius. Note that a radial from the center of curvature to the edge of the aperture is the hypotenuse of a right triangle whose other two sides are the aperture radius and an axial line segment shorter than the radius of curvature by the thickness. Symbolically,

$$d = r - \sqrt{r^2 - a_0^2} \quad (\text{B.1})$$

Next, from geometric optics [11], we know that the focal length of a planar-convex lens is related to the radius of curvature of the convex surface by

$$F_\ell = r / (n - 1) \quad (\text{B.2})$$

where, for a thick lens,  $F_\ell$  is measured from a point on the axis, inside the lens, at a distance  $d/n$  from the planar surface. With our requirement that the focal point of the lens coincide with the focal point of the horn, we have another expression for  $F_\ell$ , specifically that

$$F_\ell = 2a_0 + d/n \quad (\text{B.3})$$

Combining (B.2) and (B.3) to eliminate the focal length, we have that

$$r = (n - 1)(2a_0 + d/n) \quad (\text{B.4})$$

Finally, we solve (B.1) and (B.4) simultaneously to obtain expressions for the radius of curvature and thickness of the lens. After some algebra, we obtain  $r$  and  $d$  as functions of the aperture radius and index of refraction as

$$r = \frac{(n - 1) \left( -2n + \sqrt{n(-2 + 5n - 8n^2 + 4n^3)} \right)}{n(n - 2)} a_0 \quad (\text{B.5})$$

$$d = \frac{2n(1 - n) + \sqrt{n(-2 + 5n - 8n^2 + 4n^3)}}{n - 2} a_0$$

Thus, given the refractive index of the lens material and the desired aperture radius, the collimating lens design is fully determined.

## References

---

1. E. G. Farr and C. A. Frost, "Development of a Reflector IRA and a Solid Dielectric Lens IRA, Part II: Antenna Measurements and Signal Processing," Sensor and Simulation Note 401, October 1996.
2. E. G. Farr, Lanney M. Atchley, Donald E. Ellibee, and Larry L. Altgilbers, "A Solid Dielectric Lens Impulse Radiating Antenna Surrounded by a Cylindrical Shroud," March, 2004.
3. J. F. Aurand, "A TEM Horn Antenna with Dielectric Lens for Fast Impulse Response," *Ultra-Wideband, Short-Pulse Electromagnetics 3*, (C. E. Baum L. Carin and A. P. Stone eds.), New York, Plenum Press, 1997, pp. 113-120.
4. C. E. Baum, Low-Frequency Compensated TEM Horn, Sensor and Simulation Note 377, January 1995.
5. M. H. Vogel, "Design of Low-Frequency Compensation of an Extreme-Bandwidth TEM Horn and Lens IRA," Sensor and Simulation Note 391 April 1996.
6. E. G. Farr, "Off-Boresight Field of a Lens IRA," Sensor and Simulation Note 370, October 1994.
7. E. G. Farr and C. A. Frost, "Development of a Reflector IRA and a Solid Dielectric Lens IRA, Part I: Design, Predictions and Construction," Sensor and Simulation Note 396, April 1996.
8. C. E. Baum, "Impedances and Field Distributions for Parallel Plate Transmission Line Simulators," Sensor and Simulation Note 21, 6 Jun 66, Air Force Weapons Laboratory, p. 25.
9. F. C. Yang and K. S. H. Lee, "Impedance of a Two-Conical-Plate Transmission Line," Sensor and Simulation Note 221, Nov 76, Dikewood Corp., p. 27.
10. E. G. Farr, "Optimization of the Feed Impedance of Impulse Radiating Antennas Part II: TEM Horns and Lens IRAs," Sensor and Simulation Note 384, Nov 1995, Farr Research, Inc., p. 22.
11. E. Hecht and A. Zajac, *Optics*, Reading, Massachusetts, 1975, Chapter 6, p. 168.